Available online at www.sciencedirect.com
ScienceDirect
International Journal of Multiphase Flow 33 (2007) 1126–1139
International Journal of Multiphase Flow
www.elsevier.com/locate/ijmulflow

A fractal analysis of subcooled flow boiling heat transfer

Boqi Xiao [a,b], Boming Yu [a,*]

[a] Department of Physics, Huazhong University of Science and Technology, 1037 Luoyu Road, Wuhan 430074, Hubei, PR China
[b] Department of Physics and Electromechanical Engineering, Sanming University, 25 Jingdong Road, Sanming 365004, Fujian, PR China

Received 18 July 2006; received in revised form 8 April 2007

Abstract

A fractal model for the subcooled flow boiling heat transfer is proposed in this paper. The analytical expressions for the subcooled flow boiling heat transfer are derived based on the fractal distribution of nucleation sites on boiling surfaces. The proposed fractal model for the subcooled flow boiling heat transfer is found to be a function of wall superheat, liquid subcooling, bulk velocity of fluid (or Reynolds number), fractal dimension, the minimum and maximum active cavity size, the contact angle and physical properties of fluid. No additional/new empirical constant is introduced, and the proposed model contains less empirical constants than the conventional models. The proposed model takes into account all the possible mechanisms for subcooled flow boiling heat transfer. The model predictions are compared with the existing experimental data, and fair agreement between the model predictions and experimental data is found for different bulk flow rates.

Keywords: Subcooled flow boiling; Fractal; Heat transfer

1. Introduction

The subcooled flow boiling is widely applied in engineering and technology. In the development of modern cooling systems such as internal combustion engines, power engineering, nuclear reactors and microprocessors, the increasing output of specific power combined with a most compact space and weight saving design leads to high thermal loads on heating surfaces. For such devices, a high coolant power is to be required with limitations on the available surface area and the mass flux of liquid coolant as well as the acceptable wall temperature, and a controlled operating mode to the boiling regime is desirable.

In subcooled flow boiling heat transfer it is generally recognized that there are three main mechanisms contributing to the wall heat flux (q_W): single-phase heat transfer (q_{sp}), micro-layer evaporation (q_{ev}), and the

* Corresponding author.
E-mail address: yuboming2003@yahoo.com.cn (B. Yu).

0301-9322/$ - see front matter
doi:10.1016/j.ijmultiphaseflow.2007.05.001

sensible heat of fluid that occupies the volume evacuated by a departing bubble (q_b). Thus the wall heat flux can be expressed as

$$q_W = q_{sp} + q_{ev} + q_b \tag{1}$$

Bowring (1962) obtained the relation between q_{ev} and q_b as

$$\varepsilon = q_b/q_{ev} \tag{2}$$

The evaporation heat flux (q_{ev}) was given by

$$q_{ev} = \rho_G h_L V_b f N_a \tag{3}$$

where V_b is the volume of single bubble at departure, f is the bubble departure frequency, N_a is the number of active sites per unit area of heated surfaces, h_L is latent heat of evaporation of liquid, and ρ_G is the vapor density. The ratio ε is found empirically, which was given by the following expression:

$$\varepsilon = 1 + 3.2\frac{\rho c_p \Delta T_{sub}}{\rho_G h_L} \quad 1\times10^5\ \text{Pa} \leqslant p \leqslant 9.5\times10^5\ \text{Pa} \tag{4a}$$

$$\varepsilon = 2.3 \quad 9.5\times10^5\ \text{Pa} \leqslant p \leqslant 50\times10^5\ \text{Pa} \tag{4b}$$

$$\varepsilon = 2.6 \quad p \geqslant 50\times10^5\ \text{Pa} \tag{4c}$$

where p is pressure, ρ is the liquid density, c_p is specific heat at constant pressure, ΔT_{sub} is the subcooling ($T_S - T_L$) of liquid, and T_S is the saturation temperature of liquid, T_L is the bulk temperature of liquid.

The single-phase heat transfer (q_{sp}) is given by Mikic and Rohsenow (1969) as

$$q_{sp} = (1 - KN_a\pi D_b^2)h(T_W - T_L) \tag{5}$$

where K is the proportional constant for bubble diameter of influence, which is taken to be 1.8 by Judd and Hwang (1976), D_b is bubble departure diameter, T_W is the wall temperature, and h is the single-phase heat transfer coefficient for forced convection, which can be calculated using the Dittus–Boelter equation (1930)

$$h = 0.023Re^{0.8}Pr^{0.4}\left(\frac{k_L}{D}\right) \tag{6}$$

where D is the inner diameter of flow channel, k_L is thermal conductivity of liquid, Pr is the Prandtl number of fluid defined by $Pr = v/\alpha$, Re is the Reynolds number defined by $Re = uD/v$, and v is kinematic viscosity of fluid, α is thermal diffusivity of fluid, u is the bulk velocity of fluid.

As discussed by Basu et al. (2002, 2005a,b), a quantitative prediction of subcooled flow boiling heat flux from a superheated wall based on Eqs. (1)–(6) requires the knowledge of several additional empirical constants because each of the quantities D_b (or V_b), f and N_a contains several empirical constants, which usually have no physical meanings. On the other hand, the calculation of subcooled flow boiling heat transfer so far lacks the consensus as to which set of empirical constants is to be used since different authors used different correlations. Until now no united mechanistic model is available because boiling is a very complex and elusive process. From the earlier literature review of the available models for prediction of wall heat flux in flow boiling, it is evident that in most cases not all the mechanisms have been taken into account. Some studies ignored the contribution of heat transfer due to liquid circulation caused by bubbles disrupting the boundary layer and only considered q_{sp} and q_{ev} as the sum of the wall heat flux. The models by Larsen and Tong (1969), Ahmad (1970), Hancox and Nicol (1971), Maroti (1977), Lahey (1978), Chatoorgoon et al. (1992), Zeitoun (1994) fall into the above category. Most of them do not calculate q_{ev} directly, but indirectly by knowing q_W and calculating q_{sp}. In most studies some models were developed as a part of the modeling for void fraction, the independent validation of q_W partitioning has never been carried out though the overall model validation for void fraction prediction has been justified. Since most of these correlations were developed at high pressures and high velocity conditions, at low pressures the comparison on the above models with experimental data shows great discrepancies.

From the above brief review it is seen that a mechanistic model has not yet been developed, in which every component of wall heat flux should be determined independently. The modeling should be such that the

empirical relations used represent the physical process of subcooled flow boiling phenomena. In this paper, we attempt to develop a mechanistic model for subcooled flow boiling based on the fractal characteristics of sizes of active cavities on heated surfaces, and on the available relations that the volume of single bubble at departure and the bubble release frequency are related to active sizes.

2. Fractal characters of nucleation sites on boiling surfaces for subcooled flow boiling

This work is devoted to deriving a subcooled flow boiling model based on the fractal distribution of nucleation sites N_a on heated surfaces. We consider the active cavities formed on the heated surface are analogous to pores in porous media. Yu and Cheng (2002a) found that the cumulative number (N) of pores in porous media with the diameter greater than and equal to a particular value, D_s, obeys the following fractal scaling law:

$$N(D_L \geqslant D_s) = (D_{s,max}/D_s)^{d_f} \quad \text{with} \quad D_{s,min} \leqslant D_s \leqslant D_{s,max} \tag{7a}$$

where $D_{s,max}$ is the maximum diameter of pores in porous media, $D_{s,min}$ is the minimum diameter of pores in porous media, D_s is the diameter of a pore, and d_f is the fractal dimension. If active cavities formed on the heated surface are analogous to pores in pores media, the cumulative number of active cavities with diameters greater than and equal to D_c can also be described by Eq. (7a) with N and D_s replaced by N_a and D_c respectively, i.e.,

$$N_a(D_L \geqslant D_c) = (D_{c,max}/D_c)^{d_f} \quad \text{with} \quad D_{c,min} \leqslant D_c \leqslant D_{c,max} \tag{7b}$$

where D_c is the diameter of a active cavity, $D_{c,max}$ and $D_{c,min}$ are respectively the maximum and minimum diameters of active cavity. The total number of nucleation sites ($N_{a,tot}$) per unit area from the minimum active cavity to the maximum active cavity can be obtained from Eq. (7b) as

$$N_{a,tot} = \left(\frac{D_{c,max}}{D_{c,min}}\right)^{d_f} \tag{8}$$

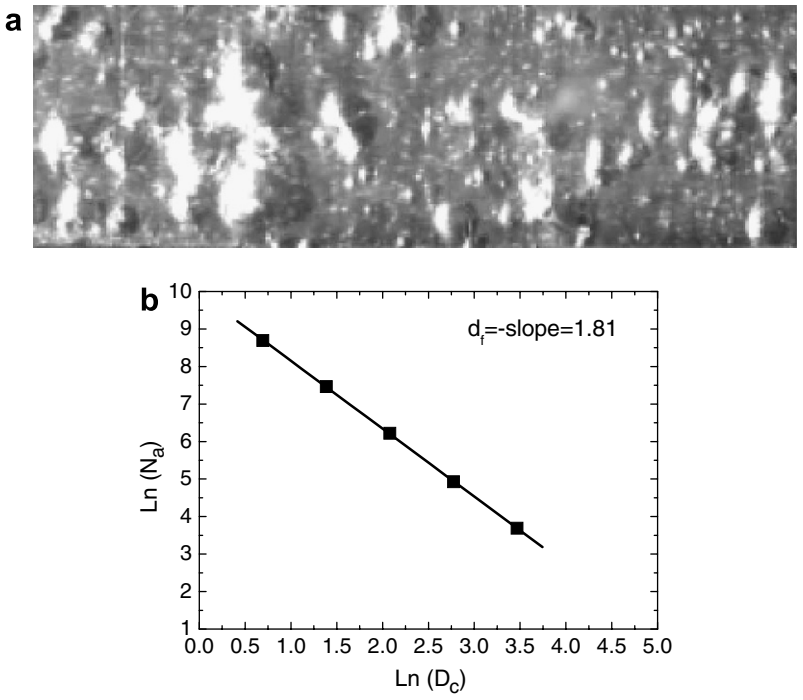

Fig. 1. (a) An image photograph (Chang et al., 2002) of active nucleation sites (white spots in the figure) at $G = 2000\ \text{kg/m}^2\,\text{s}$, $\phi = 38°$, $\Delta T_{sub} = 42.7°$, and $\Delta T_W = 29\ °\text{C}$, and (b) determination of fractal dimension of nucleation sites from (a) by the box-counting method.

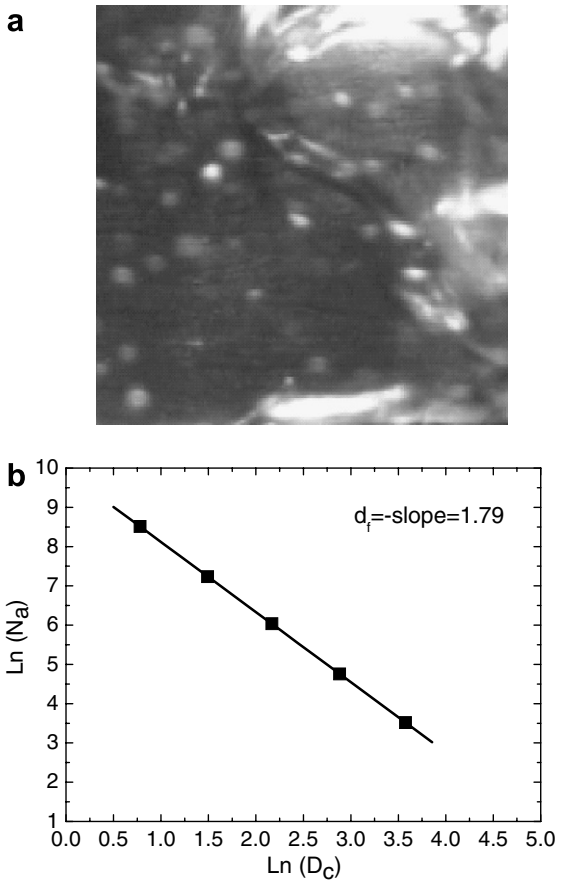

Fig. 2. (a) An image photograph (Chang et al., 2002) of active nucleation sites (white spots in the figure) at $G = 2000\ \mathrm{kg/m^2\ s}$, $\phi = 38°$, $\Delta T_{sub} = 43.1\ °C$, and $\Delta T_W = 29\ °C$, and (b) determination of fractal dimension of nucleation sites from (a) by the box-counting method.

The minimum active cavity radius R_{min} and the maximum active cavity radius R_{max} are given by Hsu (1962) for nucleation site distribution:

$$R_{min} = \frac{\delta}{C_1}\left[1 - \frac{\theta_S}{\theta_W} - \sqrt{\left(1 - \frac{\theta_S}{\theta_W}\right)^2 - \frac{4\zeta C_3}{\delta\theta_W}}\right] \tag{9a}$$

$$R_{max} = \frac{\delta}{C_1}\left[1 - \frac{\theta_S}{\theta_W} + \sqrt{\left(1 - \frac{\theta_S}{\theta_W}\right)^2 - \frac{4\zeta C_3}{\delta\theta_W}}\right] \tag{9b}$$

For subcooled flow boiling, $\theta_W = T_W - T_L = T_W - T_S + T_S - T_L = \Delta T_W + \Delta T_{sub}$, $\theta_S = T_S - T_L = \Delta T_{sub}$, and ΔT_W is wall superheat ($T_W - T_S$). So the minimum active cavity radius R_{min} and the maximum active cavity radius R_{max} can be predicted from Eq. (9) for subcooled flow boiling as

$$R_{min} = \frac{\delta}{C_1}\left[1 - \frac{\Delta T_{sub}}{\Delta T_W + \Delta T_{sub}} - \sqrt{\left(1 - \frac{\Delta T_{sub}}{\Delta T_W + \Delta T_{sub}}\right)^2 - \frac{4\zeta C_3}{\delta(\Delta T_W + \Delta T_{sub})}}\right] \tag{10a}$$

$$R_{max} = \frac{\delta}{C_1}\left[1 - \frac{\Delta T_{sub}}{\Delta T_W + \Delta T_{sub}} + \sqrt{\left(1 - \frac{\Delta T_{sub}}{\Delta T_W + \Delta T_{sub}}\right)^2 - \frac{4\zeta C_3}{\delta(\Delta T_W + \Delta T_{sub})}}\right] \tag{10b}$$

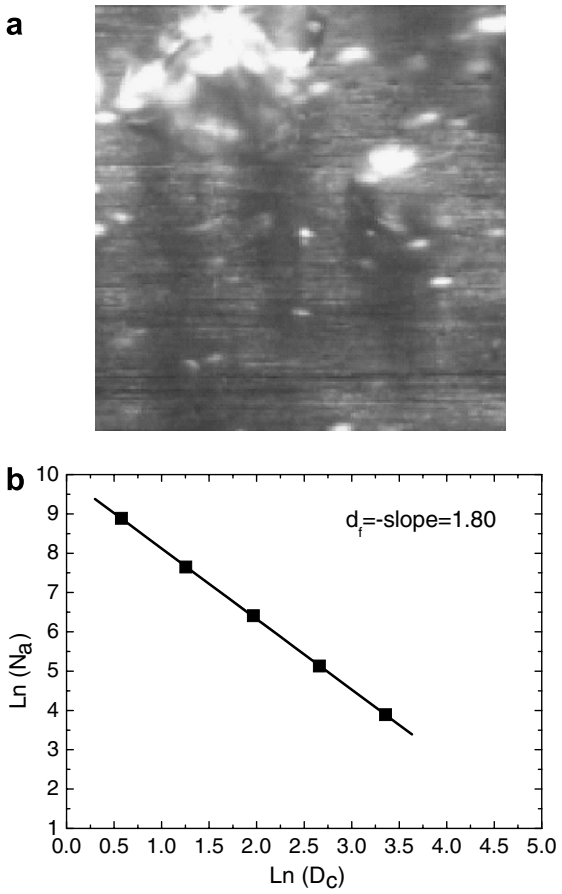

Fig. 3. (a) An image photograph (Chang et al., 2002) of active nucleation sites (white spots in the figure) at $G = 2000\ \mathrm{kg/m^2\ s}$, $\phi = 38°$, $\Delta T_{\mathrm{sub}} = 41.6\ °\mathrm{C}$, and $\Delta T_{\mathrm{W}} = 29\ °\mathrm{C}$, and (b) determination of fractal dimension of nucleation sites from (a) by the box-counting method.

where $\zeta = \frac{2\sigma T_{\mathrm{S}}}{\rho_{\mathrm{G}} h_{\mathrm{L}}}$, $C_1 = \frac{(1+\cos\phi)}{\sin\phi}$ and $C_3 = 1 + \cos\phi$, with ϕ being the contact angle of the fluid and the heater material, and σ is surface tension of fluid. δ is the thermal boundary layer thickness which can be usually expressed as

$$\delta = \frac{k_{\mathrm{L}}}{h} \tag{11}$$

where h is the single-phase heat transfer coefficient for forced convection, which is calculated by Eq. (6).

For a boiling system, the fractal dimension d_{f} of nucleation sites is given by Yu and Cheng (2002b) as

$$d_{\mathrm{f}} = \frac{\ln\left[\frac{1}{2}\left(\frac{\overline{D}_{\mathrm{c,max}}}{D_{\mathrm{c,min}}}\right)^2\right]}{\ln\frac{D_{\mathrm{c,max}}}{D_{\mathrm{c,min}}}} \tag{12}$$

where $\overline{D}_{\mathrm{c,\,max}}$ is the averaged value over all the maximum active cavities as

$$\overline{D}_{\mathrm{c,max}} = \frac{1}{(T_{\mathrm{W}} - T_{\mathrm{S}})}\int_{T_{\mathrm{S}}}^{T_{\mathrm{W}}} D_{\mathrm{c,max}}(T_{\mathrm{W}})\mathrm{d}T_{\mathrm{W}} = \frac{1}{\Delta T_{\mathrm{W}}}\sum_{j=1}^{m} D_{\mathrm{c,max}}(T_{\mathrm{W}_j})\delta T_{\mathrm{W}} = \frac{1}{m}\sum_{j=1}^{m} D_{\mathrm{c,max}}(T_{\mathrm{W}_j}) \tag{13}$$

where $m = \Delta T_{\mathrm{W}}/\delta T_{\mathrm{W}}$, and a constant δT_{W} is assumed. In the above equation, $T_{W_j} = T_{\mathrm{S}} + j(\delta T_{\mathrm{W}})$ with $j = 1, 2, \ldots, m$. For example, if we choose $\delta T_{\mathrm{W}} = 0.2\ °\mathrm{C}$ then $m = 5$ for $\Delta T_{\mathrm{W}} = 1\ °\mathrm{C}$, and $m = 50$ for $\Delta T_{\mathrm{W}} = 10\ °\mathrm{C}$.

Table 1
A comparison on the fractal dimensions between the present model predictions by Eq. (12) and the Box-counting method applied to the experimental data by Chang et al. (2002) at pressure $p = 1.13 \times 10^5$ Pa and mass flux $G = 2000$ (kg/m^2 s)

Case no.	q_W (MW/m^2)	ΔT_{sub} (°C)	Method and model predictions	d_f
1	6.1	42.7	Box-counting method for Fig. 1a	1.81
			Prediction by Eq. (12)	1.84
2	5.8	43.1	Box-counting method for Fig. 2a	1.79
			Prediction by Eq. (12)	1.79
3	7.0	41.6	Box-counting method for Fig. 3a	1.80
			Prediction by Eq. (12)	1.81

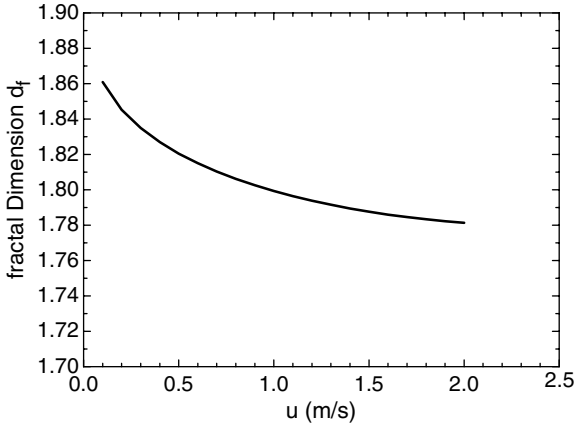

Fig. 4. Fractal dimension versus the bulk velocity of liquid at $p = 1.013 \times 10^5$ Pa, $T_S = 100$ °C, $\Delta T_{sub} = 10$ °C, $\Delta T_W = 25$ °C, and $\phi = 38°$.

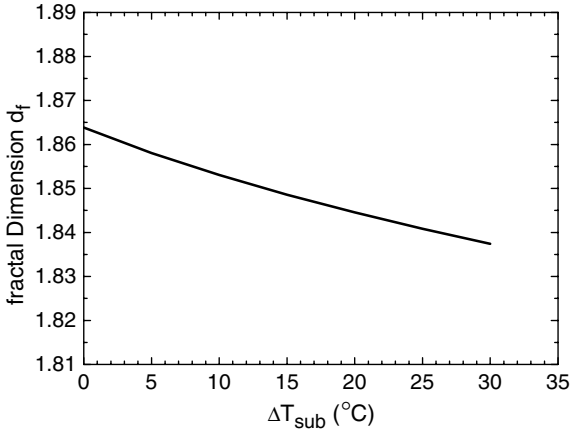

Fig. 5. Fractal dimension versus subcooling at $p = 1.013 \times 10^5$ Pa, $T_S = 100$ °C, $\Delta T_W = 20$ °C, $u = 0.1$ m/s and $\phi = 38°$.

Figs. 1a, 2a and 3a are three photo images from the reference by Chang et al. (2002) for nucleation sites in subcooled flow boiling experiments. A vertical, one-side heated rectangular channel was used as test section. The experimental conditions were the following: $p = 1.13 \times 10^5$ Pa, $G = 2000$ kg/m^2 s (mass flux), $T_S = 103$ °C, $\Delta T_{sub} = 42.7$ °C, and $q_W = 6.1$ MW/m^2 for Fig. 1a; $T_S = 103$ °C, $\Delta T_{sub} = 43.1$ °C, and $q_W = 5.8$ MW/m^2 for Fig. 2a; $T_S = 103$ °C, $\Delta T_{sub} = 41.6$ °C, and $q_W = 7.0$ MW/m^2 for Fig. 3a. A linear relationship on the log–log coordinate can be obtained as shown in Figs. 1b, 2b and 3b after the box-counting

method (Feder, 1988) was applied to the image photos. A comparison on the fractal dimensions between the present model predictions by Eq. (12) and the box-counting method applied to the image photos is summarized in Table 1. It can be seen from Table 1 that the error are about 1.7% (Fig. 1a), 0.1% (Fig. 2a) and 0.6% (Fig. 3a). This confirms that the nucleation sites follow the fractal scaling law given by Eq. (7).

Fig. 4 is a plot of the fractal dimension (d_f) versus the bulk velocity (u) of liquid at $p = 1.013 \times 10^5$ Pa, $T_S = 100$ °C, $\Delta T_W = 25$ °C, $\Delta T_{sub} = 10$ °C, and $\phi = 38°$. Fig. 4 shows that the fractal dimension decreases as the bulk velocity of liquid increases. This is expected because the high bulk velocity may cause the reduction of the total number of nucleate sites and thus reduces the fractal dimension.

Fig. 5 is a plot of the fractal dimension (d_f) versus subcooling (ΔT_{sub}) at $p = 1.013 \times 10^5$ Pa, $T_S = 100$ °C, $\Delta T_W = 20$ °C, $u = 0.1$ m/s and $\phi = 38°$. The figure denotes that the smaller the ΔT_{sub}, the larger the fractal dimension d_f. This can be explained that the smaller subcooling (ΔT_{sub}) means that the bulk temperature of liquid is close to the saturation temperature of liquid, leading to the more nucleate sites and thus higher fractal dimension.

Fig. 6 shows a comparison on the $N_{a,tot}$ values versus ΔT_W for three different contact angles at $p = 1.013 \times 10^5$ Pa, $T_S = 100$ °C, $\Delta T_{sub} = 2$ °C and $u = 0.01$ m/s. It can be seen from Fig. 6 that the active nucleation site density increases with ΔT_W. An increase in either ΔT_W or ϕ results in an increase in $N_{a,tot}$. This can be explained that the high wall superheat or the large contact angel causes the increase of nucleate sites, leading to the more bubbles on heated surfaces.

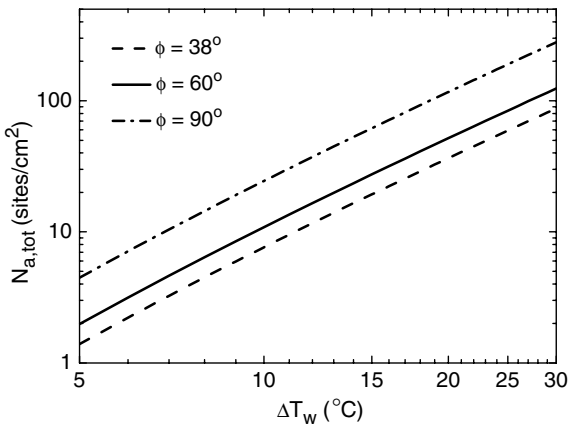

Fig. 6. A comparison of $N_{a,tot}$ for different contact angles at $p = 1.013 \times 10^5$ Pa, $T_S = 100$ °C, $\Delta T_{sub} = 2$ °C and $u = 0.01$ m/s.

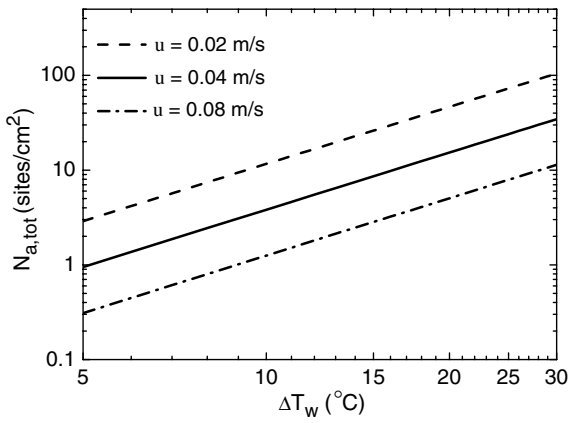

Fig. 7. A comparison of $N_{a,tot}$ for different bulk velocities of liquid at $p = 1.013 \times 10^5$ Pa, $T_S = 100$ °C, $\Delta T_{sub} = 0$ °C, and $\phi = 90°$.

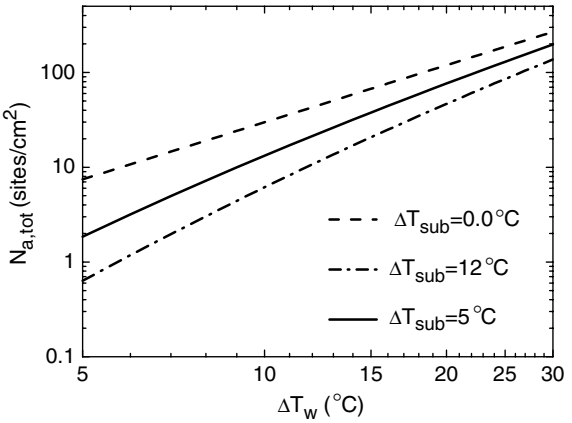

Fig. 8. A comparison of $N_{a,tot}$ for different liquid subcoolings at $p = 1.013 \times 10^5$ Pa, $T_S = 100$ °C, $u = 0.01$ m/s, and $\phi = 85°$.

Fig. 7 compares the total nucleate sites $N_{a,tot}$ versus ΔT_W for three different bulk velocities of liquid at $p = 1.013 \times 10^5$ Pa, $T_S = 100$ °C, $\Delta T_{sub} = 0$ °C, and $\phi = 90°$. It is again seen that the total number of nucleate sites decreases with the increase of bulk velocity, but increases linearly with the increase of ΔT_W. This is consistent with physical phenomena. Fig. 8 compares the $N_{a,tot}$ values at three different values of ΔT_{sub} at $p = 1.013 \times 10^5$ Pa, $T_S = 100$ °C, $u = 0.01$ m/s, and $\phi = 85°$. It can be seen that a decrease in ΔT_{sub} results in an increase in $N_{a,tot}$. This indicates that the more nucleate sites are activated and become bubbles on heated surfaces at smaller ΔT_{sub}, which is consistent with physical phenomena.

3. Fractal model for subcooled flow boiling

In the following, a fractal model for subcooled flow boiling is derived based on the fact that the nucleation site size distribution follows the fractal power law given by Eq. (7b). The number of active cavities of sizes lying between D_c and $D_c + dD_c$ can be obtained from Eq. (7b) as

$$-dN_a = d_f D_{c,max}^{d_f} D_c^{-(d_f+1)}\, dD_c \tag{14}$$

where $dD_c > 0$ and $-dN_a > 0$. Eq. (14) indicates that the nucleation site number decreases with the increase of diameter of active cavity.

Conventionally, N_a in Eq. (3) is related to the active cavity diameter or heat flux by a variety of correlations with several empirical constants. However, no generally accepted model for N_a has been available so far. This work attempts to modify Eq. (3) and derive a fractal model for heat flux from evaporation (q_{ev}). Since the size distribution of nucleation sizes is found to be fractal, a fractal model for heat flux from evaporation (q_{ev}) from the minimum site $D_{c,min}$ to the maximum site $D_{c,max}$ can be obtained by modifying Eq. (3) as

$$q_{ev} = \int dq_{ev} = \int_{D_{c,min}}^{D_{c,max}} \rho_G h_L V_b f(-dN_a) \tag{15}$$

where f is the bubble release frequency and V_b is the volume of single bubble at departure. Both f and V_b are also related to the nucleation site size D_c and will be discussed later, and $(-dN_a)$ is given by Eq. (14). Eq. (15) indicates that the heat flux from evaporation (q_{ev}) depends on the active site sizes, the bubble departure frequency f as well as the volume V_b of single bubble at departure. The higher the number of active sites, the higher the heat flux q_{ev}; the higher the bubble departure frequency f, the higher the heat flux q_{ev}; and the larger the volume V_b of single bubble at departure, the higher the heat flux q_{ev}. These are expected and are consistent with the practical situations. Eq. (15) can be integrated if the bubble departure diameter f and the volume V_b of single bubble at departure are expressed in terms of D_c. The volume V_b of single bubble at departure is given by Van der Geld (1996) as

$$V_b = \frac{\pi D_c^3}{Eo} \tag{16a}$$

where Eo is Eotvos number, which is given by Mori and Baines (2001) as

$$Eo = \frac{g(\rho - \rho_G)D_c^2}{\sigma} \tag{16b}$$

where g is gravitational acceleration. If Eq. (16b) is substituted into Eq. (16a), the volume V_b of single bubble at departure can be obtained from Eq. (16a) as

$$V_b = \frac{\pi\sigma}{g(\rho - \rho_G)} D_c \tag{17}$$

It is evident that volume V_b of a single bubble at departure is proportional to the active cavity D_c and fluid properties. Eq. (17) denotes that the larger the active cavity D_c, the larger the volume V_b of single bubble at departure. This can be explained that the larger the active cavity D_c means the larger bubble diameter at departure, leading to the larger volume V_b of a single bubble at departure.

We note that the bubble departure frequency, f, is usually expressed as

$$f = \frac{1}{t_w + t_g} \tag{18}$$

where t_w is the bubble waiting time, t_g is the bubble growth time. In pure liquids, Van Stralen et al. (1975) assumed that the waiting time is related to the growth time by

$$t_w = 3t_g \tag{19}$$

Han and Griffith (1965) obtained the analytical expression for the bubble waiting time, t_w, which is related to the cavity size ($D_c = 2R_c$) by

$$t_w = \frac{9}{4\pi\alpha}\left[\frac{(T_W - T_L)R_c}{T_W - T_S[1 + (2\sigma/R_c\rho_G h_L)]}\right]^2 \tag{20}$$

where R_c is the cavity radius. On a copper surface, Wang and Dhir (1993) measured $R_c = 1.1$–27.7 μm at 1 atm pressure. A rough estimation of the term $2\sigma/R_c\rho_G h_L$ gives 0.1–0.01 for $R_c = 1.0$–10 μm. So in Eq. (20) the term $2\sigma/R_c\rho_G h_L$ can be neglected for the simplicity of integration, since $T_W - T_L = \Delta T_{sub} + \Delta T_W$ and $T_W - T_S = \Delta T_W$ for subooled flow boiling, and Eq. (20) can be further reduced to

$$t_w = \frac{9}{4\pi\alpha}\left[\frac{(T_W - T_L)D_c}{2(T_W - T_S)}\right]^2 = \frac{9D_c^2(\Delta T_W + \Delta T_{sub})^2}{16\pi\alpha(\Delta T_W)^2} \tag{21}$$

Eq. (21) indicates that the larger the active cavity or the higher subcooling, the longer the waiting time. This is consistent with the physical phenomena. Substituting Eqs. (21) and (19) into Eq. (18), we can see that the bubble departure frequency, f, is related to the sizes of active cavities as

$$f = \frac{4\pi\alpha(\Delta T_W)^2}{3(\Delta T_W + \Delta T_{sub})^2} D_c^{-2} \tag{22}$$

From Eqs. (17) and (22) we see that both the volume V_b of single bubble at departure and the bubble departure frequency f are related to the sizes of active cavities. So Eq. (15) can now be integrated to give

$$\begin{aligned} q_{ev} &= \int_{D_{c,min}}^{D_{c,max}} \rho_G h_L V_b f(-dN_a) \\ &= \int_{D_{c,min}}^{D_{c,max}} \frac{4\pi^2}{3}\rho_G h_L \alpha \frac{\sigma}{g(\rho - \rho_G)}\left(\frac{\Delta T_W}{\Delta T_W + \Delta T_{sub}}\right)^2 D_c^{-1} d_f D_{c,max}^{d_f} D_c^{-(d_f+1)}\, dD_c \\ &= c_{ev}\frac{d_f}{d_f + 1}\left(\frac{\Delta T_W}{\Delta T_W + \Delta T_{sub}}\right)^2 \left[D_{c,max}^{d_f} D_{c,min}^{-d_f-1} - D_{c,max}^{-1}\right] \end{aligned} \tag{23a}$$

where $C_{ev} = \frac{4\pi^2 \rho_G h_L \sigma \alpha}{3g(\rho - \rho_G)}$, which is independent of cavity sizes. Eq. (23a) denotes that the heat flux from evaporation is a function of wall superheat, liquid subcooling, bulk velocity of fluid (or Reynolds number) and fractal dimension, the minimum and maximum active cavity size, the contact angle and physical properties of fluid, and no additional/new empirical constant is introduced in this model. It is expected that Eq. (23a) has less empirical constants than the conventional models, and every parameter in Eq. (23a) has clear physical meaning. Eq. (23a) shows that the heat flux from evaporation can be determined independently, but indirectly by knowing q_W and calculating q_{sp} in the conventional models.

With the aid of Eqs. (8) and (23a) can be rewritten as

$$q_{ev} = c_{ev} \frac{d_f}{d_f + 1} \left(\frac{\Delta T_W}{\Delta T_W + \Delta T_{sub}} \right)^2 D_{c,max}^{-1} \left[(N_{a,tot})^{1+1/d_f} - 1 \right] \tag{23b}$$

which indicates that the heat flux from evaporation is proportional to the total number of nucleation sites per unit area and inversely proportional to the maximum diameter of nucleation site. Since $N_{a,tot} \gg 1$, Eq. (23b) can be further reduced to

$$q_{ev} = c_{ev} \frac{d_f}{d_f + 1} \left(\frac{\Delta T_W}{\Delta T_W + \Delta T_{sub}} \right)^2 D_{c,max}^{-1} N_{a,tot}^{1+1/d_f} \tag{23c}$$

Yu and Cheng (2002b) compared the pore sizes in porous media to the sizes of nucleation sites and obtained the following expression:

$$\psi = \left(\frac{D_{c,min}}{D_{c,max}} \right)^{d - d_f} \tag{24}$$

where ψ is volumetric (or area) fraction, and $d = 2$ in the two-dimensional space for heated surfaces. Eq. (24) can be applied to describe the volume (area) fraction of nucleation sites (see the white spots in Figs. 1a, 2a and 3a). Due to $T_W - T_L = \Delta T_{sub} + \Delta T_W$, a fractal model for single-phase heat flux (q_{sp}) can be obtained by modifying Eq. (5) as

$$\begin{aligned} q_{sp} &= (1 - K\psi) h (T_W - T_L) = \left[1 - K \left(\frac{D_{c,min}}{D_{c,max}} \right)^{2 - d_f} \right] h (\Delta T_{sub} + \Delta T_W) \\ &= \left[1 - K (N_{a,tot})^{1 - 2/d_f} \right] h (\Delta T_{sub} + \Delta T_W) \end{aligned} \tag{25}$$

Eq. (25) denotes that the single-phase heat flux (q_{sp}) is a function of wall superheat, liquid subcooling, bulk velocity of fluid (or Reynolds number), fractal dimension, the minimum and maximum active cavity sizes, the contact angle and the single-phase heat transfer coefficient. Eq. (25) shows that the single-phase heat flux can be computed independently, but indirectly by knowing q_W in the conventional models.

Inserting Eqs. (23) and (25) into Eq. (1), we obtain a fractal model for the wall heat flux as

$$\begin{aligned} q_W &= q_{sp} + q_{ev} + q_b = q_{sp} + (1 + \varepsilon) q_{ev} \\ &= \left[1 - K \left(\frac{D_{c,min}}{D_{c,max}} \right)^{2 - d_f} \right] h (\Delta T_{sub} + \Delta T_W) + (1 + \varepsilon) c_{ev} \\ &\quad \times \frac{d_f}{d_f + 1} \left(\frac{\Delta T_W}{\Delta T_W + \Delta T_{sub}} \right)^2 \left[D_{c,max}^{d_f} D_{c,min}^{-d_f - 1} - D_{c,max}^{-1} \right] \\ &= \left[1 - K (N_{a,tot})^{1 - 2/d_f} \right] h (\Delta T_{sub} + \Delta T_W) + (1 + \varepsilon) c_{ev} \frac{d_f}{d_f + 1} \left(\frac{\Delta T_W}{\Delta T_W + \Delta T_{sub}} \right)^2 D_{c,max}^{-1} N_{a,tot}^{1+1/d_f} \end{aligned} \tag{26}$$

where $D_{c,min}$ and $D_{c,max}$ are given by Eq. (10) h is given by Eq. (6), ε is determined by Eq. (4) according to different pressures, d_f is obtained from Eq. (12), $N_{a,tot}$ is calculated by Eq. (8), $C_{ev} = \frac{4\pi^2 \rho_G h_L \sigma \alpha}{3g(\rho - \rho_G)}$ is independent of cavity sizes. Eq. (26) depicts that the wall heat flux is a function of wall superheat, fluid subcooling, bulk velocity of fluid (or Reynolds number), fractal dimension, the total number of nucleation sites, the minimum and maximum active cavity sizes, the contact angle and physical properties of fluid, and no additional/new

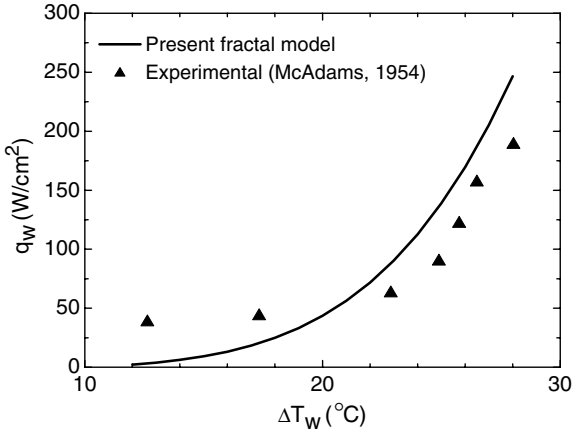

Fig. 9. A comparison between the model prediction and experimental data (McAdams, 1954) from the subcooled flow boiling at $p = 4.13 \times 10^5$ Pa, $G = 1104$ kg/m^2 s, $\Delta T_{sub} = 27.8$ °C and $\phi = 38°$.

empirical constant is introduced in this model. It is expected that Eq. (26) has less empirical constants than conventional models, and every parameter in Eq. (26) has clear physical meaning. This fractal model has taken

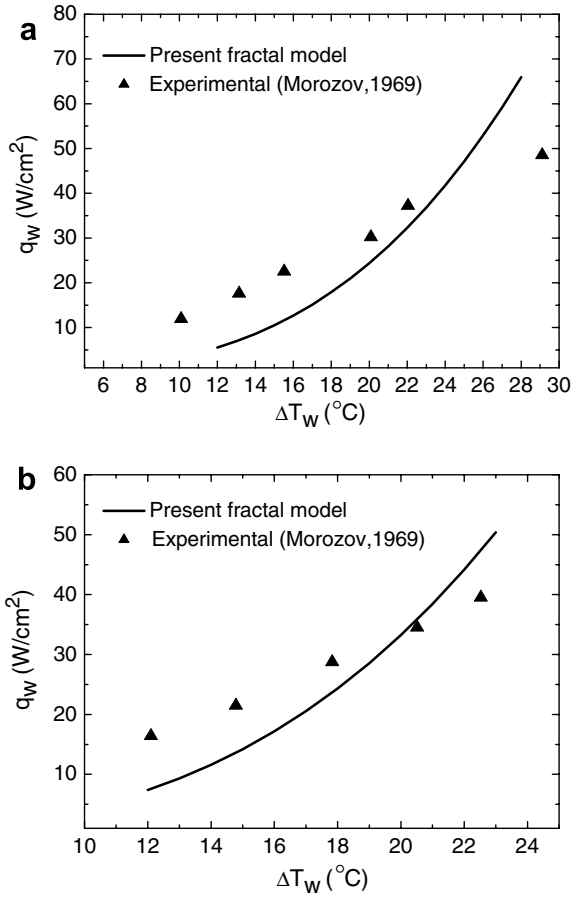

Fig. 10. (a) A comparison between the present model predictions and the experimental data (Morozov, 1969) at $p = 31 \times 10^5$ Pa, $G = 819$ kg/m^2 s, $\Delta T_{sub} = 0$ °C and $\phi = 38°$, and (b) a comparison between the present model predictions and the experimental data (Morozov, 1969) at $p = 41.4 \times 10^5$ Pa, $G = 795$ kg/m^2 s, $\Delta T_{sub} = 0$ °C and $\phi = 38°$.

into account all the possible mechanisms and included q_{sp}, q_b and q_{ev}. But in conventional models some studies ignored the contribution by q_b. In this model, q_{ev}, q_b and q_{sp} are calculated directly and may be applicable at low pressures and low bulk flow rates, whereas most of conventional models are applicable only at high pressures and high velocities.

4. Comparison with heat flux data for subcooled flow boiling

Fig. 9 compares the model predictions with the experimental data by McAdams (1954), who conducted the subcooled flow boiling experiments on a stainless steel surface at pressure $p = 4.13 \times 10^5$ Pa, $G = 1104$ kg/m^2 s, $\Delta T_{sub} = 27.8$ °C and $\phi = 38°$. It is seen that fair agreement is observed between the model predictions and the experimental data. The solid line in Fig. 9 represents the predictions by the present fractal model with

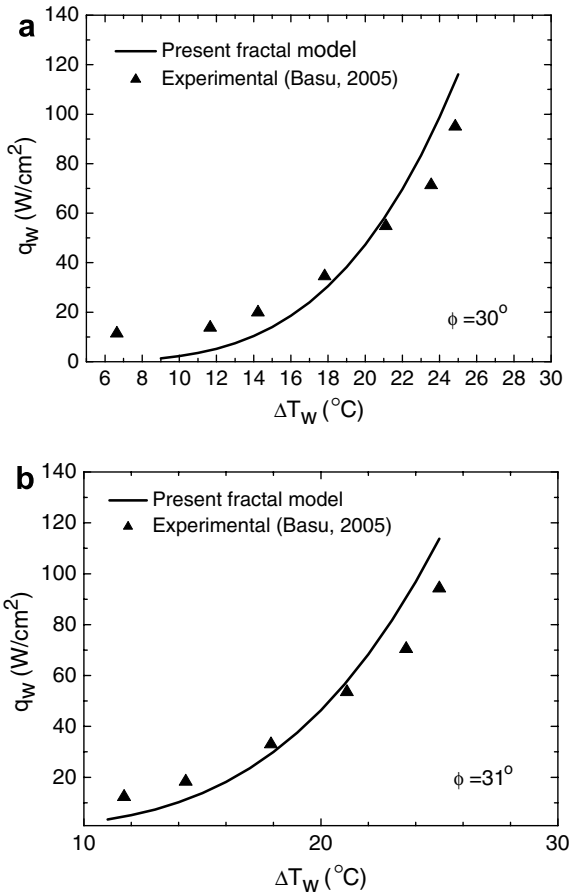

Fig. 11. A comparison between the present model predictions and the experimental data (Basu et al., 2005b) at $p = 1.03 \times 10^5$ Pa, $G = 346$ kg/m^2 s, $\Delta T_{sub} = 7.4$ °C, $\phi = 30°$ and $\phi = 31°$, respectively.

Table 2
A comparison between the present model predictions and the experimental data (Basu et al., 2002) at $P = 1.03 \times 10^5$, $\phi = 90°$ and $G = 346$ kg/m^2 s

Comparisons	ΔT_{sub} (°C)	ΔT_w (°C)	q_w (W/cm^2)
Experimental data	10.2–12.9	9.2–23.5	16.0–94.4
Model predictions	10.2–12.9	14–22	15.5–106

the value of d_f computed from Eq. (12). The maximal error may reach 40%, when the wall superheat is in the range of 17.3 °C $\leqslant \Delta T_W \leqslant$ 28 °C, see Fig. 9.

Morozov (1969) also conducted experiments on a stainless steel surface at 31×10^5–41×10^5 *Pa* for water boiling. In the literature since the contact angle was not given, the contact angle of 38° was used, which is a typical value for water boiling on a stainless steel surface. Fig. 10a shows a comparison between the model predictions and experimental data at $p = 31 \times 10^5$ Pa. The maximal error may reach 43% when the wall superheat is in the range of 15.5 °C $\leqslant \Delta T_W \leqslant$ 22 °C, see Fig. 10a. While Fig. 10b shows a comparison at $p = 41.4 \times 10^5$ Pa. Fair agreement is also observed between the experimental and predicted values from Fig. 10b. The maximal error may reach 15% when the wall superheat is in the range of 17.8 °C $\leqslant \Delta T_W \leqslant$ 22.3 °C, see Fig. 10b.

Fig. 11a and b compare our model predictions with Basu et al. (2005b)'s experimental data on the vertical Copper plate at pressure $p = 1.03 \times 10^5$ Pa, $G = 346$ kg/m^2 s, $\Delta T_{sub} = 7.4$ °C, $\phi = 30°$ and $\phi = 31°$, respectively. It is seen that fair agreement between the model predictions and the experimental data is again found. The maximal error may reach 28% when the wall superheat is in the range of 11.7 °C $\leqslant \Delta T_W \leqslant$ 25 °C, see Fig. 11a. While The maximal error may reach 29% when the wall superheat is in the range of 11.8 °C $\leqslant \Delta T_W \leqslant$ 25.3 °C, see Fig. 11b.

Table 2 summarizes that the comparison between the present model predictions and experimental data by Basu et al. (2002). It is seen from Table 2 that good agreement between our model predictions and the experimental data is found.

5. Summary and conclusion

A fractal model for the subcooled flow boiling is derived based on the fractal distribution of active nucleation sites on boiling surfaces. The proposed model is expressed as a function of wall superheat, liquid subcooling, bulk velocity of fluid (or Reynolds number), fractal dimension, the minimum and maximum active cavity sizes, the contact angle and physical properties of fluid. No additional/new empirical constant is introduced, and the proposed model contains less empirical constants than the conventional models. The present fractal model takes into account all the possible mechanisms for subcooled flow boiling heat transfer. The predicted wall heat flux based on the proposed fractal model has been shown in fair agreement with experiment data. The validity of the present fractal model is thus verified.

Acknowledgement

This work was supported by the National Natural Science Foundation of China through Grant No.10572052.

References

Ahmad, S.Y., 1970. Axial distribution of bulk temperature and void fraction in a heater channel with inlet subcooling. ASME J. Heat Transfer 92, 595–609.

Basu, N., Warrier, G.R., Dhir, V.K., 2002. Onset of nucleate boiling and active nucleation site density during subcooled flow boiling. ASME. J. Heat Mass Transfer 124, 717–728.

Basu, N., Warrier, G.R., Dhir, V.K., 2005a. Wall heat flux partitioning during subcooled flow boiling – Part I: model development. ASME. J. Heat Mass Transfer 127, 131–140.

Basu, N., Warrier, G.R., Dhir, V.K., 2005b. Wall heat flux partitioning during subcooled flow boiling – Part II: model validation. ASME. J. Heat Mass Transfer 127, 141–148.

Bowring, R.W., 1962. Physical model based on bubble detachment and calculation of steam voidage in the subcooled region of a heated channel, HPR-10. Institutt for Atomenergi, Halden, Norway.

Chang, S.H., Bang, I.C., Baek, W-P., 2002. A photographic study on the near-wall bubble behavior in subcooled flow boiling. Int. J. Therm. Sci. 41, 609–618.

Chatoorgoon, V., Dimmick, G.R., Garver, M.B., Selander, W.N., Shoukri, M., 1992. Application of generation and condensation models to predict subcooled boiling void at low pressures. Nucl. Technol. 98, 366–378.

Dittus, W.F., Boelter, L.M.K., 1930. University of California Publication on Engineering, vol. 2, Berkeley, CA, p. 443.

Feder, J., 1988. Fractals. Plenum Press, New York.

Han, C.Y., Griffith, P., 1965. The mechanism of heat transfer in nucleate pool boiling – Parts I and II. Int. J. Heat Mass Transfer 8, 887–913.

Hancox, W.T., Nicol, W.B., 1971. A general technique for the prediction of void distributions in non-steady two-phase forced convection. Int. J. Heat Mass Transfer 14, 1377–1394.

Hsu, Y.Y., 1962. On the size range of active nucleation cavities on a heating surface. J. Heat Transfer 84, 207–215.

Judd, R.L., Hwang, K.S., 1976. A comprehensive model for nucleate pool boiling heat transfer including microlayer evaporation. Int. J. Heat Mass Transfer 98, 623–629.

Lahey, R.T., 1978. A mechanistic subcooled boiling model. In: Proceedings of the 6th International Heat Transfer Conference, pp. 293–297.

Larsen, P.S., Tong, L.S., 1969. Void fractions in subcooled flow boiling. ASME Journal of Heat Transfer 91, 471–476.

Maroti, L., 1977. Axial distribution of void fraction in subcooled boiling. Nucl. Technol. 34, 8–17.

McAdams, W.H., 1954. Heat Transmission. McGraw-Hill, New Work.

Mikic, B.B., Rohsenow, W.M., 1969. A new correlation of pool boiling data including the effect of heating surface characteristic. Trans. ASME. J. Heat Mass Transfer 91, 245–250.

Mori, Brian K., Baines, W. Douglas, 2001. Bubble departure from cavities. Int. J. Heat Mass Transfer 44, 771–783.

Morozov, V.G., 1969. Convective heat transfer in two phase flow. In: Borishannskii, V.M., Paleev, I.I., (Eds.), Israel Program for Scientific Transactions.

Van der Geld, C.W.M., 1996. Bubble detachment criteria: some criticism of 'Das Abreissen von Dampfblasen an festen Heizflachen'. Int. J. Heat Mass Transfer 39, 653–657.

Van Stralen, S.J.D., Sohan, M.S., Cole, R., Sluyter, W.M., 1975. Bubbles growth rates in pure and binary systems: combined effect of relaxation and evaporation microlayers. Int. J. Heat Transfer 18, 453–467.

Wang, C.H., Dhir, V.K., 1993. Effect of surface wettability on active nucleation site density during pool boiling of water on a vertical surface. ASME J. Heat Transfer 115, 659–669.

Yu, B.M., Cheng, P., 2002a. Fractal models for the effective thermal conductivity of bidispersed porous media. AIAA J. Thermophys. Heat Transfer 16, 22–29.

Yu, B.M., Cheng, P., 2002b. A fractal model for nucleate pool boiling heat transfer. ASME J. Heat Transfer 124, 1117–1124.

Zeitoun, O., 1994. Subcooled flow boiling and condensation, Ph.D. thesis. McMaster University, Hamilton, Ontario, Canada.